CHEMISTRY OF MATERIALS

ARTICLE

pubs.acs.org/cm

Direct SECM Localized Electrografting of Vinylic Monomers on a Conducting Substrate

Federico Grisotto, Achraf Ghorbal,† Cédric Goyer, Julienne Charlier,* and Serge Palacin

DSM/IRAMIS/SPCSI CEA-Saclay, 91191 Gif-sur-Yvette Cedex (France)

Supporting Information

ABSTRACT: Localized electrografting of vinylic monomers in aqueous solution with micrometer resolution has been accomplished using scanning electrochemical microscopy (SECM). The SECM device was used in the direct mode, where the substrate acted as the cathodic working electrode and the ultramicroelectrode (UME) served as the anodic counter electrode in a classical three-electrode cell arrangement. The localized effect appeared when the protons reduction regime was obtained at the conducting substrate and in the same time when the oxidation of water was achieved at the UME. The different factors that determine the size and pattern of the electrografted coating were examined. The localization of the coatings, which were characterized by infrared spectroscopy in the reflection−absorption mode (IRAS), X-ray photoelectron spectroscopy (XPS), atomic force microscopy (AFM), and optical microscopy, was interpreted in terms of transportation modes of the reactive species, mainly supported by the migration effect rather than the diffusion effect. We have also demonstrated that the UME in the environment of a SECM device can be used as a pencil to direct the electrografting of organic film, which is of great interest for chemical, biological, or technical applications.

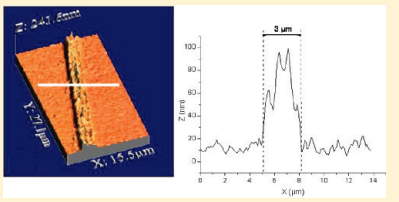

KEYWORDS: electrografting, electrochemical lithography, patterning, surface functionalization

1. INTRODUCTION

Modified surfaces containing spatially defined functionalities are a desirable goal for numerous applications. Recent years have seen considerable progress in the development of microfabricated systems for use in the chemical and biological sciences. Existing approaches typically expose macroscopic areas of a substrate to milliliter quantities of solution to attach one type of molecule, sometimes using light and specialized chemistry to carry out localized reactions.[1−7] Thus, localized addressing can be obtained under electronic or photochemical radiation,[8] using microrobotic pipetting of microdroplets,[9] via a two-dimensional electrophoretic technique,[10] with a printing technique by microcontact.[11−15] Most of these techniques require multiple-step processes and their implementation is usually tedious and expensive. Because of the requirement of a continuous scaling down, technologies and systems should be miniaturized to close the recent gap between microtechnology and nanotechnology. Therefore, microsystems must be continuously developed.

In this context, the objective of our work is to develop an inexpensive and mask-free technique by combining local probes techniques (scanning electrochemical microscopy, SECM) and electrografting processes in view of tuning locally chemical and physical surface properties on initially homogeneous substrates.

SECM, which is one of the major developments in the field of electrochemistry in the past decade, has been shown to be a promising analytical tool for localized studies of surface reactions and their kinetics, for imaging at the microscale or nanoscale level and for local surface modifications. Since its introduction by Bard et al.[16,17] and Engström et al.,[18,19] SECM has mainly been used to image surface topography and electrochemical topography. We will also report on several recent reviews (Sun et al.,[20] Edwards et al.,[21] and Amemiya et al.[22]) for a very comprehensive overview of its general application and theory, as well as its use in current research.

Early in the development of the SECM, it was recognized that, when an ultramicroelectrode (UME) is brought near a conducting surface, electron transfer is confined to a small area on the surface. So, SECM-based surface patterning can be used to form a variety of micrometer-sized structures. For example, SECM has been widely used for the patterning of insulating substrates,[23−27] the deposition of polymers[28−30] and metals,[31] and the etching processes of metals and semiconductors, as well as for the local modification of various target surfaces,[32,33] the local deposition of gold, and further functionalization by thiolates.[34] However, electrografting via the direct mode has been rarely evoked even if, very recently, the direct mode has been used to induce the grafting of conducting surfaces with organic layers.[35,36] Nevertheless, except for the electrodeposition of large 10-μm domains of conducting polymers such as polypyrrole,[37,38] it generally consists of the electrochemical transformation of self-assembling monolayers (SAMs).[39] It must be highlighted that, with SECM, no preformed stamp or mask is needed prior to patterning the substrate, since the pattern is formed by scanning the UME; in addition, the micrometer-sized delimitations of the deposited

Received: June 4, 2010
Revised: February 3, 2011
Published: February 24, 2011

pattern fulfill a basic need for most of the microfabrication techniques.

So, to the best of our knowledge, the potential of a local conducting probe to induce, electrochemically, a nonconducting micrometer-sized patterned polymer film (called electrografting) in the direct mode on a conducting substrate have not yet been developed with SECM. Moreover, it must be highlighted that, in our direct-mode configuration, the substrate plays the role of the working electrode while the UME acts as the auxiliary one, which represents a rarely used configuration for the direct mode. The present work is related to this point. To avoid any misunderstanding, it must be clearly noted that our work does not want to be a contribution to the theoretical and/or instrumental development of the SECM technique itself. Our objective is clearly to use SECM as an electrochemical tool to allow us to generate locally particular electrochemical conditions able to start the grafting process. For that reason, we attempted to rationalize our observations in terms of basic electrochemical processes and gather enough experimental evidence and interpretations to provide a convincing proof of concept.

Recently, we described the successful cathodic polymerization of vinylic monomers in aqueous solution on metal substrates using initiators, such as aryldiazonium salts.[40−42] The aryldiazonium salts can indeed be easily reduced at low cathodic reduction potential to generate free radicals that eventually initiate the polymerization of the vinylic monomers. The process, which is called surface-electroinitiated emulsion polymerization (SEEP), proved efficient both for water-soluble vinylic monomers in aqueous conditions and for lipophilic monomers in emulsion conditions.

Among the three steps of the grafting process (see Supporting Information 1 for the detailed mechanism), only the first one is likely to be sensitive to the current lines, which are orthogonal to the ohmic isopotentials. In contrast, the growth of the polymer film is radical-type and, therefore, is poorly influenced by the electric field. However, we can expect that the radical species involved in the growth of the polymer film are actually sensitive to the diffusional field resulting in changes of concentration in the vicinity of the electrodes. Moreover, it is established that the reduction of protons plays a crucial role for the growth of the polymer.[43] This phenomenon should also contribute to localize the grafting.

2. EXPERIMENTAL SECTION

SECM Experiments. Experiments were performed on a SECM370 unit (Uniscan Instruments) in a one-compartment Teflon cell. The electrografting process was carried out with a standard three-electrode arrangement. The working electrodes were microscope glass slides coated with 2 nm of chromium and 100 nm of gold (99.99%) via vacuum evaporation. The reference electrode was a pseudo-reference Ag wire (Φ = 1 mm) and the UMEs acted as counterelectrodes in the electrical circuit. The Pt microdisk electrodes were prepared according to the literature (see Supporting Information A for a brief description of the UMEs' fabrication).[44−46] The tip was moved using a horizontal and vertical translation stage that was driven by an electric microstep engine. Potential and current were imposed or measured via a bipotentiostat coupled with the SECM370 workstation. The z-approach curves (see Figure A in the Supporting Information) and the $X-Y$ planarity checking of the sample were realized by setting the microelectrode potential on the reduction plateau of $Fe(CN)_6^{3-}$ (5×10^{-3} mol dm^{-3}, KCl 0.1 mol dm^{-3}). After the alignment process, the ferrocyanide solution was pumped off and, after the cell was rinsed with ultrapure water, replaced by the electrolytic solution.

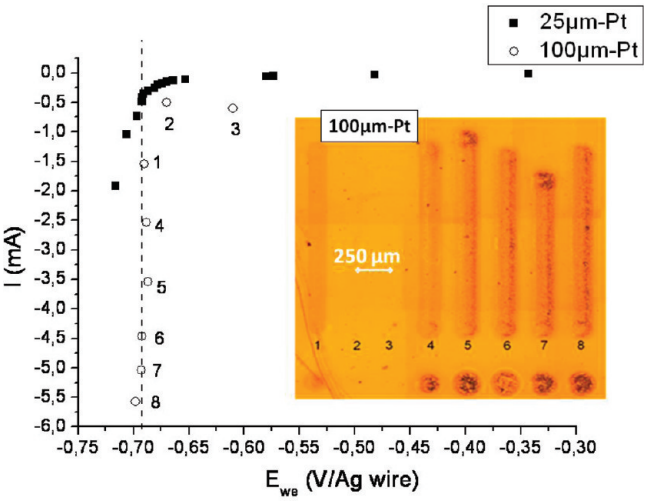

Figure 1. $I(E)$ curves reconstructed from the recorded E_{we} value during chronopotentiometry experiments with different applied current values ((■) 25-μm Pt UME and (○) 100-μm Pt UME). (Conditions: d/a = 0.6, t = 5 s.) Dashed line represetns the onset of the proton reduction regime. Inset: optical microscopy images of the localized grafting as a function of the applied current for the 100-μm Pt UME.

The electrolytic medium was made of commercial acrylic acid (AA) (Aldrich) in acidic aqueous solution (H_2SO_4, 0.25 mol dm^{-3}, analytical grade) in the presence of 4-nitrobenzenediazonium tetrafluoroborate (DNB) (Aldrich, 2×10^{-3} mol dm^{-3}). The electro-initiated polymerization technique consists of applying chronoamperometric or chronopotentiometric technique. The SECM tool was used either in static mode to make dots or in dynamic mode to draw lines. All the samples were sonicated in ethanol and water before any analyses to remove any ungrafted matter.

Characterization. The localization of the organic grafts was observed by optical microscopy (Leica DMLM with CDD camera Leica DFC 320) and atomic force microscopy (AFM) in contact mode (Molecular Imaging PicoLe). The AFM data were treated with the WSxM software.[47] The samples were also analyzed by X-ray photoelectron spectroscopy (XPS) (Kratos Axis Ultra DLD, Al Kα monochromatic source) and infrared spectroscopy in the reflection−absorption mode (IRAS) (Bruker IFS66, coupled with a HYPERION 3000 microscope). The latter techniques both have single-point measurements, line maps, area maps, and imaging capabilities. The grafted polymer has characteristic spectroscopic features that can be used as a probe to trace the growth of the polymer on the surface.

3. RESULTS AND DISCUSSION

Proof of Concept. Figure 1 shows the evolution of the potential for the working electrode (E_{we}), as a function of the current imposed on the substrate when the 25-μm Pt UME or the 100-μm Pt UME counterelectrode was placed at a normalized working distance (i.e., the ratio between the working distance d and the tip radius a (d/a)) equal to 0.6. If the potential experienced by the substrate was limited to the range where we observed only the reduction of the diazonium salt ($0 < E_{we} < -0.65$ V/Ag wire), no localized grafting was observed (see data 2 and 3 in the insert in Figure 1). Under these conditions, we, in fact obtained, a thin (<10 nm thick) grafted coating on the entire surface (see the Supporting Information). As shown by Figure 1,

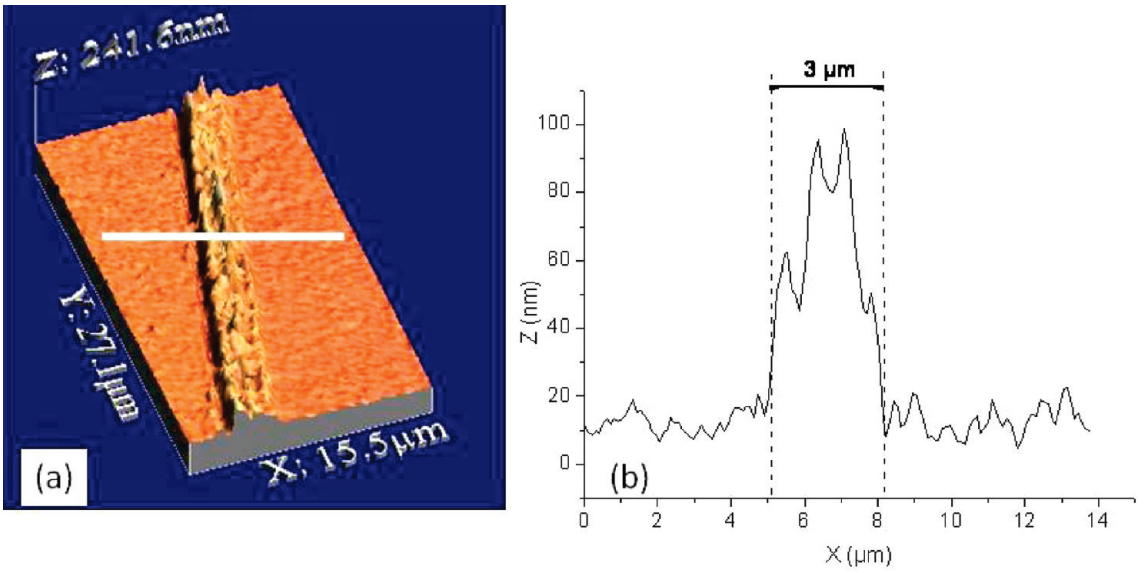

Figure 2. (a) Topographical three-dimensional (3D) AFM image of the electrografted coating obtained with 5-μm Pt UME, and (b) the AFM profile. (Conditions: [AA]: 2.0 mol dm^{-3} (where AA denotes acrylic acid); [DNB]: 2 × 10^{-3} mol dm^{-3} (where DNB denotes 4-nitrobenzenediazonium); [H_2SO_4]: 0.25 mol dm^{-3}, d/a = 1.0, I = −2 mA, v = 100 μm s^{-1}.)

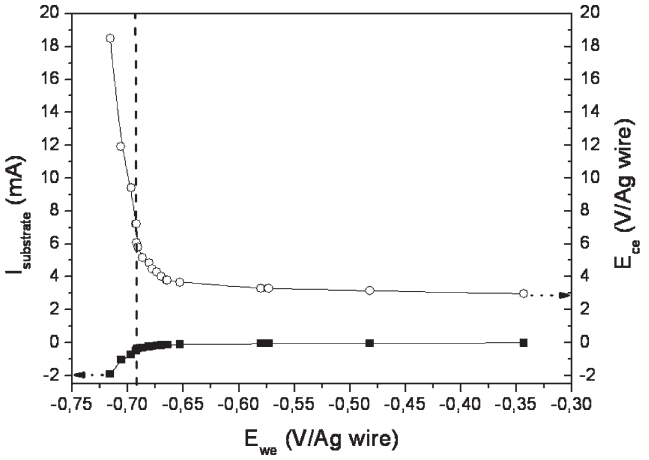

Figure 3. $I(E)$ curves reconstructed from the recorded E_{we} (square, left scale) and E_{ce} (open circle, right scale) during chronopotentiometry experiments when different current intensities were applied to the substrate. (Conditions: 25-μm Pt UME, d/a = 0.6, t = 5 s, [DNB] = 2 × 10^{-3} mol dm^{-3}, [AA] = 0.7 mol dm^{-3}, and [H_2SO_4] = 0.25 mol dm^{-3}.) Dashed line represents the onset of the proton reduction regime.

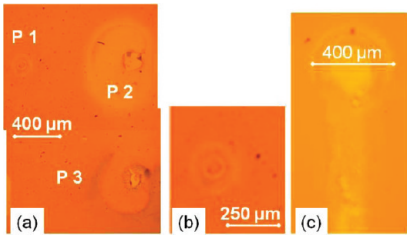

Figure 4. (a) Optical microscopy image of imprinted patterns on a gold substrate with a 50-μm Pt UME from aprotic organic solution: [BuMA] = 0.7 mol dm^{-3}, [DNB] = 2 × 10^{-3} mol dm^{-3}, [Et_4NBF_4] = 0.2 mol dm^{-3}, DMF, d/a = 0.8, t = 5 s. P1: E_{we} = −0.2 V/Ag wire; P2: E_{we} = −0.8 V/Ag wire; and P3: E_{we} = −1.2 V/Ag wire. (b) High-magnification view of the "Liesegang ring"-like pattern. (c) Optical microscopy image of imprinted pattern on gold substrate with a 100-μm Pt UME from protic organic solution. (Conditions: [AA] = 0.7 mol dm^{-3}, [DNB] = 2 × 10^{-3} mol dm^{-3}, [H_2SO_4] = 0.25 mol dm^{-3}, DMF, d/a = 0.4, E_{we}= −0.8 V/Ag wire.)

that threshold potential corresponds to a current higher (in absolute value) than −0.5 mA. Therefore, for the chronopotentiometry experiments, we selected a current in the range of −2 mA for which (i) the protons reduction regime is actually reached for all the considered UMEs, (ii) the grafted coating is homogeneous, and (iii) the coating is thick enough to be easily detected. In the insert in Figure 1, we also observe that the size of the grafted pattern does not change with the intensity of the current. However, its thickness increases with the applied current and, for the highest current range, the homogeneity of the localized coating seems affected. The experiments performed with different electrodes (ranging from 5 μm to 100 μm in diameter) resulted, in static mode, in dots patterns, the dimensions of which were proportional to the electrode diameter. In other words, smaller electrodes yield smaller patterns for the same electrolysis time and the same normalized electrode−surface distance. If the experiments were realized in dynamic mode, the best lateral resolution that we achieved in the conventional SECM environment was on the order of 3 μm with 5-μm Pt UME (see Figure 2).

It is very important to note that when the reduction of the protons occurred on the substrate, consequently, bceause of the big difference in size between both surfaces, the potential of the UME counterelectrode (E_{ce}) increased exponentially to very high values (see Figure 3), where the oxidation of water occurs with a vigorous gaseous evolution. Of course, this gaseous evolution creates a large hydrodynamic acceleration but also a quite important disturbance in the electrical field and electrochemical processes. More particularly, the bubble-dispersed phase generates a void layer that acts as an electrical shield, where the shielding effect is dependent on the density of the bubbles. There is few works concerning the local modeling of coupled electroactive species transport and electrochemical processes in a biphasic electrolyte. We were not able to evaluate

Scheme 1. Schematic View of the Different Electrochemical and Chemical Reaction Occurring on the Substrate, at the Tip, and in the Tip/Substrate Gap

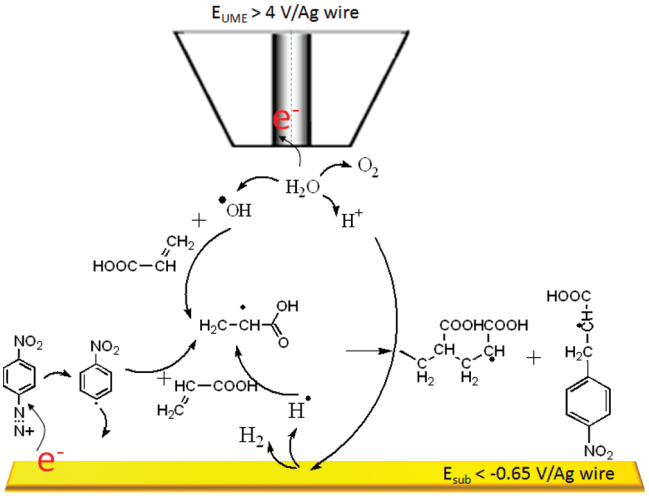

the width of the void layer in our electrochemical conditions. But, as reported in the literature, the bubble diameter ranges from 10 μm to 400 μm, depending on the current densities, the nature of the electrode, etc., ...[48−53] Therefore, this parameter would be an obvious source of perturbation, especially for the shortest working distances.

The suspected important role played by the reduction of protons and the oxidation of water on the localization of the coating can be further evidenced by reproducing the same type of experiments in an aprotic organic solvent (dimethylformamide, DMF) with a nonprotic monomer (butylmethacrylate, BuMA). Figure 4 shows an optical microscopy image of a typical spot pattern. Each spot shows inner circular centers and outer rings. Since we used a 50-μm Pt UME for patterning, the inner centers correspond to the surface area of the substrate directly below the platinum microelectrode, where the produced aryl radicals had the highest concentration close to the gold substrate, because of the short diffusion distance. The outer rings were ~100−300 μm in diameter and presumably resulted from a concentration gradient of reaction intermediates. The obtained rings resemble "Liesegang rings",[54] which are formed in reaction-diffusion systems (Figure 4b). All these results suggest that, in an aprotic organic medium, the lifetime of a radical species is longer than that under aqueous conditions, and, thus, diffusion processes control the lateral growth of the coating. Moreover, if we added protic species (diluted sulfuric acid) to the DMF medium, a poor localization effect appeared, as detected by optical microscopy (Figure 4c).

Therefore, the localized grafting process definitely seems to be related to both linked conditions: the proton reduction regime on the substrate and the consequent water oxidation on the tip. Taking into account this last point, one cannot exclude, at the tip, the formation of oxygenated species such as $O_{3(g)}$, H_2O_2, and $^{\bullet}OH$.[55] Among these species, one must pay particular attention to $^{\bullet}OH$ radicals, which is one of the strongest oxidizing agents, which can eventually oxidize organic compounds via radical mechanisms.[55,56] We can thus distinguish reactions occurring on the substrate (reduction of diazonium salt, protons, and species generated at the tip), on the tip (oxidation of water), and in the tip/substrate gap (radical reactions). Finally, it is noteworthy that O_2 gaseous evolution, which occurs at the tip during water oxidation, is associated with a void layer that must be taken into account in this Results and Discussion section. A schematic view of this scenario is represented in Scheme 1.

Before evaluating the factors that affect the size and shape of the patterns, we characterized the electrolocalized coating by infrared and XPS spectroscopies (see the Supporting Information). Infrared measurement performed on and around the disk pattern unambiguously revealed the presence of an electrografted organic coating film on the entire surface and more specifically localized on the spot, with the usual IR features of the polynitrophenylene (PNP) (1530 and 1350 cm^{-1}, corresponding to the stretching vibration of NO_2 group, and 1600 cm^{-1}, related to the phenyl group) and poly(acrylic acid) (PAA) layers (1730 cm^{-1}, characteristic of the stretching vibration of the carbonyl group). The thickness of the coating remains low outside the spot (<10 nm thick, as measured by profilometry), whereas the thickness of the localized spot (measured by AFM or profilometry) can reach several dozens of nanometers, depending on the experimental conditions. XPS mapping (400 μm × 400 μm) performed on the grafted pattern obtained with the 100-μm tip diameter, as a function of the core levels (N 1s, O 1s, C 1s), also evidenced the localization of the organic layer and confirmed the presence of both polymers. Indeed, the C 1s peak shows PNP with the peak centered at 284.8 eV attributed to the carbon double bond of phenyl groups and the PAA with the peak centered at 289 eV, assigned to acid groups (−COOH). In the N 1s region, one distinguishes a peak centered at 406 eV, which is characteristic of the NO_2 groups. The second peak at ~399 eV can be assigned to reduced nitrogen (NH_2) with its corresponding protonated form NH_3^+ (shoulder near 402 eV). The contribution at ~401 eV is attributed to azo groups (−N═N−) coming either from incomplete electroreduction of the diazonium group[57] or from a direct copulation reaction between the diazonium salt and any grafted aromatic ring in PNP. Finally, note that the O 1s core level spectrum does not correspond, quantitatively, to the sum of the expected oxygenated species (related to the detected NO_2 group and COOH group signals, respectively), and cannot be related to the eventual presence of residual sulfate ions in the grafted film (no S signal was detected). One must also take into account that such an excess is not observed when electrografting experiments are carried out in a nonlocal way, i.e., with a macroscopic counter-electrode (the potential of which never exceeds 2 V vs Ag wire during electrolysis). It is quite difficult to identify precisely the nature of the functional groups responsible for that observed excess, neither by IR nor by XPS measurements. However, OH radicals are known to react easily with aromatic rings. More particularly, hydroxyl radicals react quickly with nitro benzene molecules to form phenol moieties.[55,58,59] Therefore, we assume that the oxygenated reactive species generated under the tip react with nitrobenzene radicals (coming from the reduction of the nitrobenzene diazonium salt present in solution), thus leading to "additional" phenol moieties in the skeleton of the grafted film. The IR and XPS features of such compounds (except for the intensity of the O 1s core level signal) are not specific enough to be differentiated from the signature of the main coating.

Previous studies in our laboratory undertaken on the SEEP process demonstrated that the optimized concentration of aryl diazonium salt in the electrolytic medium for starting the process is close to 2 × 10^{-3} mol dm^{-3}.[42] Therefore, we took

dx.doi.org/10.1021/cm101563n |Chem. Mater. 2011, 23, 1396–1405

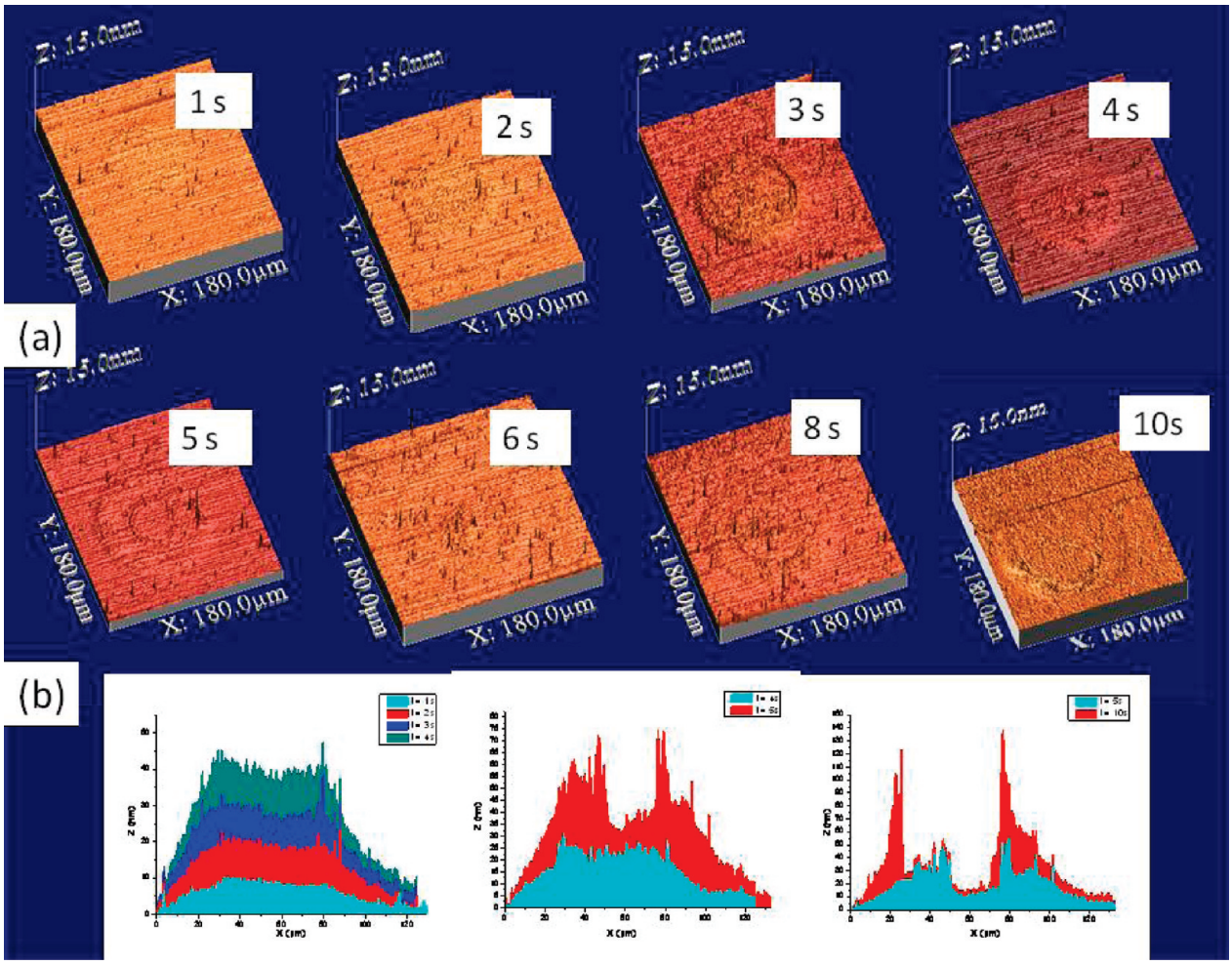

Figure 5. Evolution of the growth of the localized dot as a function of electrolysis time by AFM analysis in contact mode: (a) images in friction mode and (b) topographical AFM profiles. (Conditions: [AA] = 2.0 mol dm^{-3}, [DNB] = 2 × 10^{-3} mol dm^{-3}, [H_2SO_4] = 0.25 mol dm^{-3}, I = −2 mA, 25-μm Pt, d = 10 μm.)

that value as a constant and we studied the influence of the other parameters (such as the acrylic acid concentration, the duration of electrolysis, the working distance, and the scan rate) on the performances (lateral resolution and thickness) of the localized grafting.

Influence of the Acrylic Acid Concentration. First of all, we optimized the range of acrylic acid concentration in the electrolytic medium in view to obtain a well-localized, defined, and reproducible pattern on the substrate. We applied chronopotentiometric technique by setting the current range of the working electrode to −2 mA. Under those conditions, the potential experienced by the substrate is, whatever the acrylic acid concentration, more negative than −0.65 V vs Ag wire and thus susceptible to get localized grafting. It was found that a wide range of acrylic acid solution (0.5 mol dm^{-3} < [AA] < 7 mol dm^{-3}) can be used in view of well-resolved localized electrografting. Outside this range, the pattern is blurred. Within this range, the size of the pattern is roughly constant, whatever the AA concentration. To explain this behavior, several considerations must be taken into account.

First of all, to understand why low AA concentrations (i.e., < 0.5 mol dm^{-3}, under our experimental conditions) lead to a poorly defined localized pattern, we must report to the reaction model depicted in Scheme 1 where, in fact, the AA monomers can be considered as trappers for radicals produced in the solution, also limiting their free diffusion. This phenomenon is very similar to the "chemical lens" effect described by Borgwarth et al.[60] If the chemical reaction between the acrylic monomer and the radical generated species is fast enough, it will be spatially limited to a thin zone surrounding the tip where the two species meet. At low AA concentration, however, we can assume that the homogeneous coupling between two radicals is likely to prevail over the heterogeneous coupling with the vinylic monomer, thereby reducing the efficiency of the "chemical lens" effect ensured by the AA monomer.

Second, for high AA concentrations (i.e., >7 mol dm^{-3}, under our experimental conditions), the resistivity of the electrolytic solution increases drastically; hence, the potentials actually experienced by the electrodes is lower than expected. The electrogenerated species are thus produced in lower quantity, and, consequently, the process is less efficient.

Influence of the Time of Reaction. An important factor in the size of the deposited feature is the time that the biased UME is held close to the surface. To follow the growth of the polymer coating as a function of time, experiments were carried out with the 25-μm Pt UME to obtain localized grafting for which the size evolution can be easily followed by AFM analysis. A working distance equal to 10 μm was maintained during the entire

dx.doi.org/10.1021/cm101563n |*Chem. Mater.* 2011, 23, 1396–1405

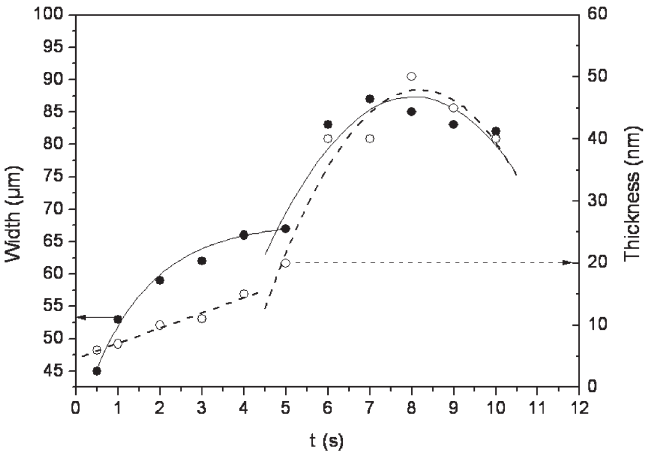

Figure 6. Evolution of the width (circle, left scale) and the thickness (open circle, right scale) of the dots pattern as a function of time. Scattered data points represent experimental data, and solid and dashed lines represent fit data. (Conditions: 25-μm Pt UME, $d = 10\ \mu$m, $I = -2$ mA, [AA] = 2.0 mol dm^{-3}, [DNB] = 2×10^{-3} mol dm^{-3}, [H_2SO_4] = 0.25 mol dm^{-3}.)

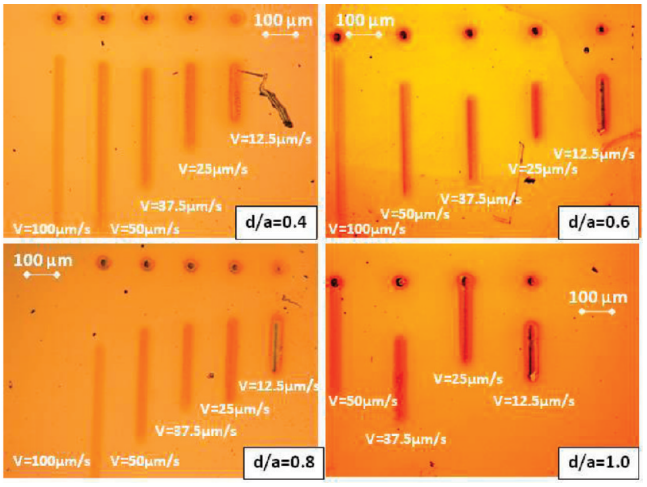

Figure 7. Example of set of experiments with a 25-μm Pt UME on a gold substrate. (Conditions: [AA] = 2.0 mol dm^{-3}, [DNB] = 2×10^{-3} mol dm^{-3}, [H_2SO_4] = 0.25 mol dm^{-3}; chronopotentiometry: $I = -2$ mA, $t = 5$ s in static mode, scan rate in dynamic mode (see graph).)

experiment. AFM images were recorded in contact mode and gathered in Figure 5. The localized coating grows radially from the center to the border, and from the profile AFM images analysis, we can extract the thickness and the width of the coating.

If we plot these data as a function of time, we clearly observe two different time regimes (see Figure 6):

(i) For $t < 5$ s, the coating rapidly reaches a roughly constant radius value ($\sim$60 μm). At the same time, its thickness increases linearly with time.

(ii) For $t \geq 5$ s, the disk pattern changes both in width and thickness. Both parameters grow slowly, following a second-order polynomial fit. Note that, at the same time, cracks appear on the top of the coating, and crack amplitude increases with time. This behavior can certainly be explained by two main reasons: (a) parasite reactions induced by the highly reactive and/or aggressive chemical environment under the UME (oxidation of water) able to ablate the growing film; (b) the high current applied on a small area of surface, able to knock off the grafting as it happens to capacitors when their dielectric material breaks.

Table 1. Average Width of the Dots Pattern, as a Function of the UME Radius

UME radius, a (μm)	width of the dot, L (μm)	$L/2a$
12.5	60 ± 10	2.4 ± 0.4
25	100 ± 10	2.0 ± 0.2
50	150 ± 10	1.5 ± 0.1

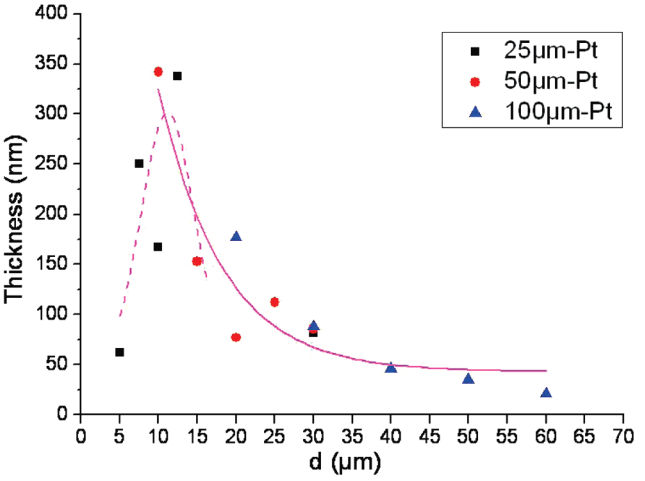

Figure 8. Thickness of the localized dots, as a function of the absolute working distance. Data points represent experimental data, dashed lines represent the Gaussian fit for $d < 10\ \mu$m, and the solid line represents the exponential decay fit for $d > 10\ \mu$m. (Conditions: [AA] = 2.0 mol dm^{-3}, [DNB] = 2×10^{-3} mol dm^{-3}, [H_2SO_4] = 0.25 mol dm^{-3}, $I = -2$ mA, $t = 5$ s.)

In conclusion, the duration of the electrolysis seems to be a valuable tool to tune the thickness of the final grafted coating. If the local coating must be thin and homogeneous (for forthcoming chemical derivatization, for example), a short time of polarization (<5 s, under our experimental conditions) must be used. In contrast, if the thickness and the roughness of the localized grafting are the sought properties, a longer time of polarization should be selected.

Influence of the Working Distance in Static Mode. To study the influence of the working distance and the scan rate of the tip, we applied the chronopotentiometric method ($I = -2$ mA) both in static and dynamic modes. For a given UME, we carried out, on the same sample, a set of experiments including, at a fixed working distance, dots and lines drawn for different scan rates. We repeated this set of experiments for different working distances. We applied this protocol for the three studied UMEs: 25- μm Pt, 50-μm Pt, and 100-μm Pt. In Figure 7, we report an example of experiments realized with the 25-μm Pt UME, for different working distances and different scan rates. The shape of the dots pattern is poorly dependent on the working distance. More precisely, the average width of the dots is constant for a given UME, whatever the working distance in the studied range ($0.2 < d/a < 2$) (see Table 1).

If our process was mainly governed by the simple diffusional phenomena, a linear dependence between the pattern diameter and the distance would be anticipated as originally discussed by

dx.doi.org/10.1021/cm101563n |*Chem. Mater.* 2011, 23, 1396–1405

Table 2. Characteristics of the Localized Coating Obtained in the Static Mode ($v = 0$), Compared to the Dynamic Mode for the Three Tested UMEs[a]

25-μm Pt UME				
v (μm s^{-1})	0	12.5	25	50
d (μm)	10	10	10	10
d/a	0.8	0.8	0.8	0.8
v/a		1	2	4
$L/2a$	2.4 ± 0.2	2.4 ± 0.2	2.4 ± 0.2	2.0 ± 0.2
thickness (nm)	167 ± 20	142 ± 20	80 ± 10	37 ± 8
50-μm Pt UME				
v (μm s^{-1})	0	10	50	100
d (μm)	10	10	10	10
d/a	0.4	0.4	0.4	0.4
v/a		0.4	2	4
$L/2a$	2.0 ± 0.2	2.1 ± 0.2	1.8 ± 0.2	1.6 ± 0.2
thickness (nm)	340 ± 20	390 ± 20	30 ± 8	22 ± 8
100-μm Pt UME				
v (μm s^{-1})	0	10	100	200
d (μm)	20	20	20	20
d/a	0.4	0.4	0.4	0.4
v/a		0.2	2	4
$L/2a$	1.5 ± 0.3	1.8 ± 0.2	1.3 ± 0.2	1.2 ± 0.2
thickness (nm)	88 ± 10	80 ± 10	18 ± 8	11 ± 8

[a] Conditions: [AA] = 2.0 mol dm^{-3}, [DNB] = 2 × 10^{-3} mol dm^{-3}, [H_2SO_4] = 0.25 mol dm^{-3}, I = −2 mA.

Bard et al.[61] Obviously, it is not the case. In fact, our electrochemical system functions as a "tip generator/substrate collector" system. The protons coming from the oxidation of the water occurring at the highly anodic-biased UME must be collected, with sufficient efficiency, on the cathodically polarized substrate for engaging the localized process. According to the model developed by Osteryoung et al.,[62,63] in the absence of a supporting electrolyte, the protons produced at the tip must migrate rather than diffuse to the substrate, where they can be reduced, to obtain a well-defined localization. The migration effect is only sensitive to the current lines, which are poorly affected by the distance between both electrodes for $0.2 < d/a < 2$.

As already mentioned above, the thickness of the grafted pattern is more sensitive to the working distance than its width. If we report the thickness of the coating as a function of the absolute value of the working distance, for all studied UMEs, we observe that the thickness of the coating reaches a maximum value for an absolute working distance of ∼10−15 μm (see Figure 8). For the very short working distances ($d < 10$ μm), the coating thickness decreases with d. For working distances of 30−40 μm, the thickness of the coating is quasi-stable and independent of the distance. For $d > 60$ μm, no localized effect is detected. To interpret these results, we should take into account the presence of a void layer near the tip resulting from the O_2 gaseous evolution. We are not able to evaluate its thickness, but we can assume that its lateral extension is related to the flux of gaseous evolution, which only depends on the potential experienced by the tip. When the working distance is very short, ($d < 10$ μm), the extension of this void layer limits the volume of the solution in contact with the substrate, thus limiting the development of the electrochemical process. When the working distance increases ($d > 10$ μm), the reaction volume in contact with the substrate increases, thus favoring the grafting process. However, at the same time, as the reaction volume increases, the electrogenerated species in the gap substrate/UME are more diluted. Therefore, we can expect that the yield of the reactions decreases with d.

Influence of the Scan Rate. If we want to lithograph a micropattern on a substrate, it is necessary to work in the dynamic mode. A new factor must be taken into account: the scan rate. Indeed, the electrode displacement introduces a convective effect that should influence the width and the thickness of the line. For the three tested UMEs, the width follows an exponential decay, as a function of the scan rate. The same behavior was observed, whatever the working distance in the range of d, where the localization is usually observed. This phenomenon is probably related to the flux convection profile of the solution in connection with the rate at which the probe is moved.[64] Therefore, the dynamic mode allows a noticeable reduction in the dimensions of the grafted pattern. We can note that, for a given working distance, the minimal width is achieved when the ratio scan rate/tip radius is equal to 2 and does not change anymore for higher speed. On the other hand, for a given scan rate, the width decreases linearly with the working distance. The thickness of the coating, as a function of the scan rate, can be fitted with an exponential decay fit for all the considered UMEs whereas, for a given working distance, the thickness decreases with the scan rate. All these graphs are available in the Supporting Information.

We can summarize these data as follows (see Table 2):

(i) The characteristics of the coatings tend toward those of the static mode when the tip is moved very slowly.

(ii) The width and the thickness of the coating depend on the time spent over one point. Shorter times (high speed) lead to narrower and thinner patterns.

(iii) The influence of the working distance on the thickness of the coating is only noticeable for the slowest displacement. When the ratio scan rate/tip radius is >2, the thickness of the coating remains more or less constant, whatever the working distance, and its value is ∼20−30 nm, whatever the tip.

It must be highlighted that working in dynamic mode allows one to graft a more homogeneous coating than in static mode. This phenomenon is probably to relate to the relative predominance of the different modes of transportation of the reactive species, i.e., migration, diffusion, and convection, into and from the reactive container, respectively. In other words, the displacement of the electrochemical reactive species is synchronized with the electrode displacement, thus improving the localization in terms of homogeneity and selectivity.

Working in dynamic mode leads to reduce not only the width but also the thickness of the coating. Therefore, a compromise that is a function of the desired applications must be found. If we need a thick, homogeneous localized coating, it will be preferable to work at a slow scan rate while we will use higher scan rates to obtain thin homogeneous graftings.

Influence of the RG Parameter. Because the UME is constituted of a metallic wire encapsulated in a glass capillary, the last parameter that should be taken into account is the RG factor (glass radius/electrode radius). To study its influence on

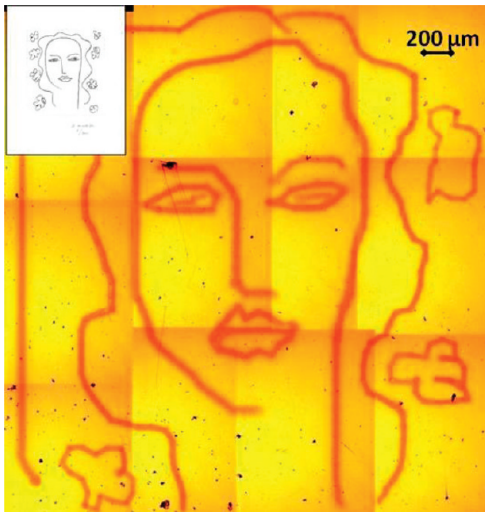

Figure 9. Reproduction of the "Madeleine" painted by Henri Matisse (inset) printed on the gold substrate by coupling SECM with Elecdraw software. (Conditions: [AA] = 2.0 mol dm^{-3}, [DNB] = 2 × 10^{-3} mol dm^{-3}, [H_2SO_4] = 0.25 mol dm^{-3}.)

the characteristics of the localized pattern, 50-μm Pt UMEs with two very different RG values (3 and 15, respectively) were prepared and characterized as usual. Localized experiments were performed in static mode by chronopotentiometry. Both electrodes present a common general behavior (see the Supporting Information), in accordance with the trends described above: i.e., (i) a lateral dimension of the dot pattern poorly influenced by the working distance in the range where the localized effect is observed; and (ii) a coating thickness that decreases with d.

However, for $d/a < 0.4$, a large RG value allows one to graft narrower and thinner patterns than a low RG value. We can assumed that a large RG value is associated with a larger void layer than a small RG value. Indeed, for a large RG value, the bubbles created at the tip have a longer journey to reach the "borders" of the tip and escape from the tip/substrate gap. Gas accumulation beneath the tip also increases the void layer and, consequently, for the shortest working distance, limits the contact area between the substrate and the tip and the development of the electrochemical process.

On the other hand, the neutral and/or radical species generated at the biased tip undergo a hemispherical diffusion process, while the ionic species, as a function of their sign, preferentially migrate to the corresponding electrode, following the current lines. The species undergoing hemispherical diffusion have a shorter journey to reach the "borders" of the tip and escape from the tip/substrate gap, when the RG value is lower. As a consequence, these species are lost for the growing of the localized coating. This effect overcomes the void layer effect for the larger working distances.

SECM as a Direct Lithographic Tool for Conducting Substrates? In collaboration with the PegasTech startup, we developed lithography software (Elecdraw1.0) that was able to drive the UME of the SECM instrument in the $X-Y$ plan above the substrate. By coupling the SECM with this software, we were thereby able to print on the substrate any complex pattern within a few minutes (see Figure 9). Some examples of grafted patterns realized with the Elecdraw software can be found in the Supporting Information. Behind the pleasant feature of this coupling, it will be very efficient as an actual lithographic tool with a micrometer resolution without using mask and lift-off technologies.

4. CONCLUSION

To summarize, we have demonstrated that the localization of electrografting is tuned by the local generation of reactive species confined to the vicinity of the UME/substrate gap. The short UME/substrate working distance limits the diffusion time of the radical species generated at the electrodes surfaces and ensures a small reaction area. However, the transportation modes are perturbed by the vigorous O_2 gaseous evolution at the tip, which creates a void layer limiting the grafting process at the shortest working distances.

The oxidation water regime, which must be achieved to observe the localization effect, has, as consequence, the production of protons, which are collected on the substrate. Therefore, our electrochemical system seems to function as a tip generator/substrate collector of reactive species. The oxidation water regime then seems to trigger the grafting with (or in complement) the diazonium reduction on the substrate.

We have observed that the surface modification of the substrate will be spatially limited to a thin zone surrounding the tip, where the reactive species meet. The vinylic monomers in the electrolyte solution and the nitrobenzene radicals electrogenerated in the medium may be playing the role of trappers, which also limit the free-radical diffusion from the solution. This phenomenon is very similar to the well-known "chemical lens" phenomenon,[60] where the diffusion of the electrodes generated species and that of the scavengers are in opposite direction.

We are quite conscious that our electrochemical environment is very complex, and it is very difficult to evaluate precisely the role played by each component of the electrolytic solution on the localized process. Moreover, most of the identified parameters are interdependent. For that reason, experiments undertaken in a four-electrode configuration where both potentials (substrate and UME) can be separately and precisely controlled are underway and will be essential to determine precisely the role played by the reactive species at each electrode.

The application of the SECM to the particular case of the grafting of vinylic monomers allows one to direct the patterning of a homogeneous conducting substrate with a covalently grafted organic coating, which one cannot obtain with conducting polymers and SAMs on gold technology. The formation of this strong interfacial bond is a key point for the properties of the final interfaces, which can then be further processed by classical methods of organic chemistry. The polyacrylate deposit may, for example, be functionalized by almost any chemically active species via a simple amidation of the carboxylic hanging groups.

We have thus demonstrated that the UME in the environment of a SECM can be used as a pencil to direct the electrografting of an organic film. The process is thus similar to dip-pen coating,[64] although the final coating is here covalently grafted as in a "classical" SEEP experiment. This new extension of the SECM/SPM techniques shows great promise for directing localized modification purposes, which is of great interest for chemical, biological, or technical applications. The present paper, which describes and explains the experimental results through chemical mechanisms, could obviously be enriched and confirmed by modeling studies, which were not within the scope of the present work.

■ ASSOCIATED CONTENT

Supporting Information. (i) SEEP mechanism, (ii) preparation and characterization of the microdisks electrodes, (iii) characterization of the localized coating, (iv) schematic representation of the electric field map, (v) evolution of the width and the thickness of the localized pattern as a function of different experimental parameters, (vi) steady-state current at Pt UME before and after localized electrografting process, and (vii) example of imprinted complex patterns. (PDF) This material is available free of charge via the Internet at http://pubs.acs.org.

■ AUTHOR INFORMATION

Corresponding Author

*Phone: + 33 1 69 08 21 49. Fax: + 33 1 69 08 64. E-mail: julienne.charlier@cea.fr.

Present Addresses

†Currently with Institut Supérieur des Science Appliquées et de Technologie of Gabès, Tunisia.

■ ACKNOWLEDGMENT

The authors gratefully thank S. Nunige, Dr. F. Kanoufi, and Dr. C. Combellas (ESPCI/LECA) for their help on the fabrication of ultramicroelectrodes and fruitful discussions. This work was supported by the National Agency of Research (ANR) through ANR-06-BLAN-0368 LOCALGRAFT project and by the C' nano Ile de France research program Locale*G*.

■ REFERENCES

(1) Fodor, S. P. A.; Leighton Read, J.; Pirrung, M. C.; Stryer, L.; Tsai Lu, A.; Solas, D. *Science* **1991**, *251*, 767.
(2) Dulcey, C. S.; Georger, J. H., Jr.; Krauthamer, V.; Stenger, D. A.; Fare, T. L.; Calvert, J. M. *Science* **1991**, *252*, 551.
(3) Stenger, D. A.; Georger, J. H.; Dulcey, C. S.; Hickman, J. J.; Rudolph, A. S.; Nielsen, T. B.; McCort, S. M.; Calvert, J. M. *J. Am. Chem. Soc.* **1992**, *114*, 8435.
(4) Singhvi, R.; Kumar, A.; Lopez, G. P.; Stephanopoulos, G. N.; Wang, D. I. C.; Whitesides, G. M.; Ingber, D. E. *Science* **1994**, *264*, 696.
(5) Sundberg, S.; Barrett, R. W.; Pirrung, M. C.; Lu, A. L.; Kiangsoontra, B.; Holmes, C. P. *J. Am. Chem. Soc.* **1995**, *117*, 12050.
(6) Tender, L. M.; Worley, R. L.; Fan, H.; Lopez, G. P. *Langmuir* **1996**, *12*, 5515.
(7) Mrksich, M.; Whitesides, G. M. *Annu. Rev. Biophys. Biomol. Struct.* **1996**, *25*, 55.
(8) Buss, G.; Schöning, M. J.; Schultze, J. W. *Electrochim. Acta* **1999**, *44*, 3899.
(9) Grzybowski, B. A.; Haag, R.; Bowden, N.; Whitesides, G. M. *Anal. Chem.* **1998**, *70*, 4645.
(10) Sreenivas, G.; Ang, S. S.; Fritsch, I.; Brown, W. D.; Gerhardt, G. A.; Woodwart, D. J. *Anal. Chem.* **1996**, *69*, 1858.
(11) Kumar, A.; Whitesides, G. M. *Appl. Phys. Lett.* **1993**, *63*, 2002.
(12) Michel, B.; Bernard, A.; Bietsch, A.; Delamarche, E.; Geissler, E.; Juncker, D.; Kind, H.; Renault, J.-P.; Rothuizen, H.; Schmid, H. *IBM J. Res. Dev.* **2001**, *45*, 697.
(13) Geissler, M.; Bernard, A.; Bietsch, A.; Schmid, H.; Michel, B.; Delamarche, E. *J. Am. Chem. Soc.* **2000**, *122*, 6303.
(14) Bernard, A.; Renault, J. P.; Michel, B.; Bosshard, H. R.; Delamarche, E. *Adv. Mater.* **2000**, *12*, 1067.
(15) Delamarche, E.; Bernard, A.; Schmid, H.; Bietsch, A.; Michel, B.; Biebuyck, H. *J. Am. Chem. Soc.* **1998**, *120*, 500.
(16) Bard, A. J.; Fan, F.-R. F.; Kwak, J.; Lev, O. *Anal. Chem.* **1989**, *61*, 132.
(17) Liu, H. Y.; Fan, F.-R. F.; Lin, C. W.; Bard, A. J. *J. Am. Chem. Soc.* **1986**, *108*, 3838.
(18) Engstrom, R. C.; Weber, M.; Wunder, D. J.; Burgess, R.; Winquist, S. *Anal. Chem.* **1986**, *58*, 844.
(19) Engstrom, R. C.; Meaney, T.; Tople, R.; Wightman, R. M. *Anal. Chem.* **1987**, *59*, 2005.
(20) Sun, P.; Laforge, F. O.; Mirkin, M. V. *Phys. Chem. Chem. Phys.* **2007**, *9*, 802.
(21) Edwards, M. A.; Martin, S.; Whitworth, A. L.; Macpherson, J. V.; Unwin, P. R. *Physiol. Meas.* **2006**, *27*, R63.
(22) Amemiya, S.; Bard, A. J.; Fan, F.-R. F.; Mirkin, M. V.; Unwin, P. R. *Annu. Rev. Anal. Chem.* **2008**, *1:4*, 1.
(23) Combellas, C.; Fuchs, A.; Kanoufi, F.; Mazouzi, D.; Nunige, S. *Polymer* **2004**, *45*, 4669.
(24) Combellas, C.; Ghilane, J.; Kanoufi, F.; Mazouzi, D. *J. Phys. Chem. B* **2004**, *108*, 6391.
(25) Combellas, C.; Kanoufi, F.; Mazouzi, D. *J. Phys. Chem. B* **2004**, *108*, 19260.
(26) Combellas, C.; Kanoufi, F.; Mazouzi, D.; Thiebault, A.; Bertrand, P.; Medard, N.; , *Polymer* **2003**, *44*.
(27) Combellas, C.; Kanoufi, F.; Mazouzi, D. *J. Electroanal. Chem.* **2006**, *589*, 243.
(28) Fortin, E.; Mailley, P.; Lacroix, L.; Szunerits, S. *Analyst* **2006**, *131*, 186.
(29) Marck, C.; Borgwarth, K.; Heinze, J. *Chem. Mater.* **2001**, *13*, 747.
(30) Zhou, J.; Wipf, D. O. *J. Electrochem. Soc.* **1997**, *144*, 1202.
(31) Heb, C.; Borgwarth, K.; Ricken, C.; Ebling, D. G.; Heinze, J. *Electrochim. Acta* **1997**, *42*, 3065.
(32) Wittstock, G.; Schuhmann, W. *Anal. Chem.* **1997**, *69*, 5059.
(33) Wihelm, T.; Wittstock, G. *Electrochim. Acta* **2001**, *47*, 275.
(34) Turyan, I.; Matsue, T.; Mandler, D. *Anal. Chem.* **2000**, *72*, 3431.
(35) Cougnon, C.; Gohier, F.; Bélanger, D.; Mauzeroll, J. *Angew. Chem., Int. Ed.* **2009**, *48*, 4006.
(36) Hauquier, F.; Matrab, T.; Kanoufi, F.; Combellas, C. *Electrochim. Acta* **2009**, *54*, 5127.
(37) Kranz, C.; Ludwig, M.; Gaub, H. E.; Schumann, W. *Adv. Mater.* **1995**, *7*, 38.
(38) Kranz, C.; Ludwig, M.; Gaub, H. E.; Schumann, W. *Adv. Mater.* **1995**, *7*, 568.
(39) Nowall, W. B.; Wipf, D. O.; Khur, W. G. *Anal. Chem.* **1998**, *70*, 2601.
(40) Deniau, G.; Azoulay, L.; Bougerolles, L.; Palacin, S. *Chem. Mater.* **2006**, *18*, 5421.
(41) Mévellec, V.; Roussel, S.; Tessier, L.; Chancolon, J.; Mayne-L'Hermite, M.; Deniau, G.; Viel, P.; Palacin, S. *Chem. Mater.* **2007**, *19*, 6323.
(42) Tessier, L.; Deniau, G.; Charleux, B.; Palacin, S. *Chem. Mater.* **2009**, *21*, 4261.
(43) Tessier, L.; Chancolon, J.; Alet, P.-J.; Trenggono, A.; Mayne-L'Hermite, M.; Deniau, G.; Jégou, P.; Palacin, S. *Phys. Status Solidi A* **2008**, *205*, 1412.
(44) Fan, F.-R. F.; Demaille, C. *Scanning Electrochemical Microscopy*; Bard, A. J., Mirkin, M. V. Eds.; Marcel Dekker: New York, 2001.
(45) Wightman, R. M.; Wipf, D. O. *Electroanal. Chem.* **1988**, *15*, 267.
(46) Amatore, C. *Physical Electrochemistry: Principles, Methods and Applications*; Rubinstein, I., Ed. Marcel Dekker: New York, 1995; p131.
(47) Horcas, I. *Rev. Sci. Instrum.* **2007**, *78*, 013705.
(48) LeRoy, R. L.; Janjua, M. B. I.; Renaud, R.; Leuenberger, U. *J. Electrochem. Soc.* **1979**, *126*, 1674.
(49) Lumanauw, D. Thesis, *Department of Metallurgy and Materials Science*, University of Toronto, Canada 2000.
(50) Nagai, N.; Takeuchi, M.; Nakao, M., *Proceedings of PSFVIP-4*, June 3−5, 2003, Chamonix, France.
(51) Nagai, N.; Takeuchi, M.; Kimura, T.; Oka, T. *Int. J. Hydrogen Energy* **2003**, *28*, 35.
(52) Philippe, M.; Jérôme, H.; Sebastien, B.; Gérard, P. *Electrochim. Acta* **2005**, *51*, 1140–1156.

(53) Riegel, H.; Mitrovic, J.; Stephan, K. *J. Appl. Electrochem.* **1998**, *28*, 10.
(54) Chopard, B.; Luthi, P. *Phys. Rev. Lett.* **1994**, *72*, 1384.
(55) Brillas, E.; Sires, I.; Oturan, M. A. *Chem. Rev.* **2009**, *109*, 6571.
(56) Weiss, E. Ph.D. Thesis, Paul Sabatier University, Toulouse III, France, 2006.
(57) D'Amours, M.; Bélanger, D. *J. Phys. Chem. B* **2003**, *107*, 4811.
(58) Oturan, M. A.; Pimentel, M.; Oturan, N.; Sirés, I. *Electrochim. Acta* **2008**, *54*, 173.
(59) Ozcan, A.; Sahin, Y.; Koparal, S. A.; Oturan, M. A. *Water Res.* **2008**, *42*, 2889.
(60) Borgwarth, K.; Heinze, J. *J. Electrochem. Soc.* **1999**, *146*, 3285.
(61) Bard, A. J.; Mirkin, C. A.; Unwin, P. R.; Wipf, D. O. *J. Phys. Chem.* **1992**, *96*, 1861.
(62) Xie, Y.; Osteryoung, J. G. *J. Electroanal. Chem.* **1997**, *439*, 163–171.
(63) Ciszkowska, M.; Stojek, Z.; Morris, S. E.; Osteryoung, J. G. *Anal. Chem.* **1992**, *64*, 2372–2377.
(64) Piner, R. D.; Zhu, J.; Xu, F.; Hong, S.; Mirkin, C. A. *Science* **1999**, *283*, 661.